Studying basin bifurcations in nonlinear triopoly games by using 3D visualization

Gian Italo Bischi,

University of Urbino, Italy,
`http://www.uniurb.it/,`
`mailto:bischi@econ.uniurb.it`

Lukas Mroz, and Helwig Hauser

VRVis Research Center, Vienna, Austria,
`http://www.vrvis.at/,`
`mailto:`{`mroz`|`hauser`}`@vrvis.at`

Abstract

We consider three-dimensional discrete dynamical system, obtained by the iteration of a noninvertible map of $\mathbb{R}^3$, which simulates the time evolution of an oligopoly game with three competing firms. The model is characterized by the presence of several coexisting stable equilibria, each with its own basin of attraction. In this paper we face the question of the delimitation of the basins and the detection of the global bifurcations that cause the creation of non-connected basins. This requires a study of the global properties of the 3-dimensional noninvertible map by the method of critical sets, based on the determination of the *contact bifurcations* through a systematic computer-assisted study. This requires the visualization of surfaces (the critical surfaces and the basins' boundaries) which sometimes are nested one inside the other. Enhanced graphical methods, based on *two-level volume rendering*, are employed in order to modulate the opacity of outer objects so that the contacts between the basins' boundaries and critical surfaces can be visualized. This is obtained through the realization of ad-hoc routines, which allow interactive 3D visualization.

Key words: Dynamic Games, Discrete Dynamical Systems, noninvertible maps, Computer Graphics, Volume Rendering.

1 Introduction

This paper builds on, and aims to contribute to three different literatures. First, it faces an *equilibrium selection* problem which is typically addressed in the literature on dynamic and evolutionary games with several coexisting equilibria (see e.g. [4,27,10,5]). In fact, we consider a discrete dynamical system which represents the time evolution of a Cournot oligopoly game with three competing firms (a triopoly game), recently proposed in [3], which is characterized by the existence of

several stable Nash equilibria [1] , each with its own basin of attraction. An *oligopoly* is a market structure where a few producers, each of appreciable size, produce the same good, or goods which are perfect substitutes. A Cournot oligopoly model (see [9]) is based on the assumption that each firm decides its own production in order to maximize its expected profits, and the fewness of firms gives rise to *inter-dependence*, that is, each firm must take into account the actions of the competitors in choosing its own action, because each profit also depends on the production decision of the competitor. In the original work of Cournot, as well as in many subsequent papers, suitable assumptions on the demand and cost functions ensure that a unique Nash equilibrium exists (see [5] for references). However, in many economic models multiple equilibria emerge and stability arguments are often used to select among them. If several equilibria are stable, then a situation of strategic uncertainty prevails, because the equilibrium to which the dynamic game converges depends on the initial condition. This naturally leads to the study of the basins of attraction, in order to ascertain the role of the starting conditions of the dynamic game in the selection of the final outcome. This issue is often addressed in the recent literature on dynamic and evolutionary games, where an equilibrium is reached by a dynamic adjustment process occurring when boundedly rational players play the game repeatedly, a mechanism which is often represented as a discrete dynamical system (see e.g. [4], ch.9, [27]). For the particular triopoly game considered in this paper, the problem stated above has already been addressed in [3], where it is shown that coexistence of stable steady states occurs with basins of attraction which may be nonconnected sets. As repeatedly stressed in [3], the presence of *nonconnected basins* is peculiar of noninvertible maps, but no attempts have been made in that paper in order to explain the global bifurcations that cause the creation of nonconnected basins.

This leads to the second stream to which the present paper contributes, which is related to the study of the global properties of noninvertible maps by the method of critical sets (see e.g. [14,23,2] and references therein). Indeed, it is now sufficiently well-known that the creation of nonconnected basins in one-dimensional noninvertible maps can be explained in terms of contacts between *critical points* and basins' boundaries (also called *contact bifurcations*, see [21]). In recent years, in the study of two-dimensional noninvertible maps, analogous results have been obtained by the method of *critical curves*, a two-dimensional generalization of the notion of local maxima and minima in the one-dimensional case (see e.g. [24,23,2]). Instead, the extension of these methods to the study of models involving three-dimensional noninvertible maps, like the one considered in the present paper, is an almost unexplored field. In this paper we try to use the method of *critical sets* in order to

---

[1] In a game a Nash Equilibrium is an optimal choice such that none of the firms has an incentive to deviate, since each player's strategy is the best response to the other players' predicted choices. In the dynamic game considered in this paper, where the time evolution of players' choices are obtained by the iteration of a map, the Nash equilibria are the fixed points of the map.

study the contact bifurcations which cause the creation of nonconnected basins. For maps of dimension greater than one, the explicit analytical expressions, in terms of elementary functions, of the critical sets, and of the basin boundaries involved in the contact bifurcations are generally not known. So, even for two-dimensional noninvertible maps, the methods followed in the determination of the *contact bifurcations* are based on a systematic computer-assisted study, carried out through a continuous dialog between analytic, geometric, and numerical methods, which often require a carefulusage of computer graphics. This creates some nontrivial practical problems when one tries to generalize such method to more than two dimensions. In fact, since the computer screen is two-dimensional, the visualization of objects in a phase spaces of dimension greater than two, and the detection of contacts among these objects as their shapes change, may become a very difficult task. In other words, the extension to higher-dimensional systems of the results on contact bifurcations, which gave so many interesting and promising results in the study of two-dimensional noninvertible maps, may become a very hard and challenging task, due to the difficulties met in the computer-assisted graphical visualization. In [3], two-dimensional sections are employed in order to visualize the basins of coexisting attractors, but this method is not useful to detect the occurrence of qualitative changes in the structure of the basins and the contact bifurcations which cause such changes.

This introduces the third topic, concerning the problem of visualizing objects which are of higher-dimensionality than the screen. Indeed, in our case the problem of 3D visualization also involves other difficulties, related to the fact that it is necessary to visualize objects which are nested inside other objects. This means that sophisticated graphical programs are necessary to modulate the opacity of the outer objects in order "to see through" them. Moreover, the critical sets are now two-dimensional surfaces embedded in a three-dimensional phase space, and their contacts with portions of basin boundaries, also given by two-dimensional surfaces, may be very difficult to be detected, unless the critical surfaces are represented like semi-transparent veils. In this paper some enhanced graphical methods, based on *two-level volume rendering* [15] are employed in order to visualize the attractors inside their basins, the portions of the basins of which are nested inside the basins of different attractors, and the contacts between the basins' boundaries and the critical surfaces. Indeed, the realization of ad-hoc routines, which allow interactive 3D visualization, reveals to be crucial in order to detect the occurrence and the effects of contact bifurcations.

The remainder of this paper is organized as follows. In Section 2 we recall the general notion of critical set for a noninvertible n-dimensional map and we give a qualitative description of the bifurcations which cause the creation of nonconnected basins. In Section 3 we introduce a noninvertible map whose iteration gives the time evolution of a triopoly game, and we give some results concerning the existence and the local stability of its fixed points, which represent the Nash equilibria of the game. In Section 4 we briefly describe the graphical method which is

3

at the basis of the computer program realized for the numerical study of the contact bifurcations of three-dimensional noninvertible maps. In particular, we show an exemplary bifurcation which changes the topological structure of a basin, from connected to nonconnected set, caused by a contact between a critical surface and the basin boundary. Such contacts are revealed through a nontrivial implementation of interactive two-level volume rendering graphical software.

In this paper we only give a few images, which are just snapshots of animated sequences representing the changes of the basins as some parameters are gradually changed along particular bifurcation paths in the space of the parameters. Further images, as well as the whole animated sequences, can be found at the web page correlated to this work (see [1]).

2 Critical sets and basin bifurcations for n-dimensional noninvertible maps

A map $T : \mathbb{R}^n \to \mathbb{R}^n$, defined by $p' = T(p)$, is a *noninvertible map* if it is "many-to-one", i.e. distinct points $p_1 \neq p_2$ exist which have the same image, $T(p_1) = T(p_2) = p'$. This means that several rank-1 preimages of a given point p' may exist, or, equivalently, several inverse mappings are defined, being $p_j = T_j^{-1}(p')$, $j = 1, ..., m$. So, the space $\mathbb{R}^n$ can be subdivided into regions Z_k, $k \geq 0$, whose points have k distinct $rank - 1$ preimages. Generally, as the point p' varies in $\mathbb{R}^n$, pairs of preimages appear or disappear as it crosses the boundary separating different regions. Hence, such boundaries are characterized by the presence of at least two coincident (merging) preimages. This leads to the definition of the critical sets, one of the distinguishing features of noninvertible maps [14,23]:

Definition. The *critical set CS* of a continuous map T is defined as the locus of points having at least two coincident $rank - 1$ preimages, located on a set CS_{-1} called *set of merging preimages*.

The critical set CS is the n-dimensional generalization of the notion of critical value (when it is a local minimum or maximum value) of a one-dimensional map [2], and of the notion of *critical curve LC* (from the French "Ligne Critique", following Gumowski and Mira [14]), of a noninvertible two-dimensional map. The set CS_{-1} is the generalization of the notion of critical point (when it is a local extremum point) of a one-dimensional map, and of the fold curve LC_{-1} of a two-dimensional noninvertible map. The critical set CS is generally formed by $(n - 1)$-dimensional hypersurfaces of $\mathbb{R}^n$, and portions of CS separate regions Z_k of the phase space characterized by a different number of $rank - 1$ preimages, for example Z_k and Z_{k+2} (this is the standard occurrence).

---

[2] This terminology, and notation, originates from the notion of critical points as it is used in the classical works of Julia and Fatou.
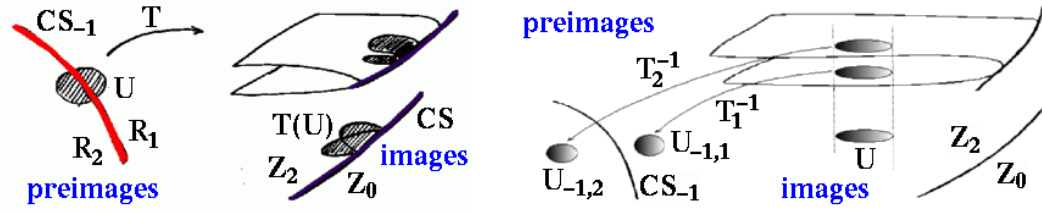
Fig. 1. Qualitative graphical illustration of the folding (on the left) and unfolding (on the right) process.

From the definition given above it is clear that the relation $CS = T(CS_{-1})$ holds, and the points of CS_{-1} in which the map is continuously differentiable are necessarily points where the Jacobian determinant vanishes:

$$CS_{-1} \subseteq J_0 = \{p \in \mathbb{R}^n \,|\, \det DT(p) = 0\} \ . \tag{1}$$

In fact, in any neighborhood of a point of CS_{-1} there are at least two distinct points which are mapped by T in the same point. Accordingly, the map is not locally invertible in points of CS_{-1}.

In order to explain the geometric meaning of the critical sets, let us consider a portion of CS, say $\widehat{CS}$, which separates two regions Z_k and Z_{k+2} of the phase space, and let $\widehat{CS}_{-1}$ be the corresponding locus of merging preimages, i.e. $\widehat{CS} = T(\widehat{CS}_{-1})$. This means that two inverses of T exist, say T_1^{-1} and T_2^{-1}, which are defined in the region Z_{k+2} (and have respective ranges in the regions R_1 and R_2 separated by $\widehat{CS}_{-1}$). Both inverses merge on $\widehat{CS}$ (i.e. they give merging preimages on $\widehat{CS}_{-1}$) and no longer exist in the region Z_k. Now, let $U \subset \mathbb{R}^n$ be a ball which intersects $\widehat{CS}_{-1}$ in $D = U \cap \widehat{CS}_{-1}$. Then $T(D) \subseteq \widehat{CS}$, and $T(U)$ is "folded" along $\widehat{CS}$ into the region Z_{k+2}. Refer to Fig. 1 for a graphical illustration. In fact, considering the two portions of U separated by $\widehat{CS}_{-1}$, say $U_1 \in R_1$ and $U_2 \in R_2$, we have that $T(U_1) \cap T(U_2)$ is a nonempty set included in the region Z_{k+2}, which is the region whose points p' have rank-1 preimages $p_1 = T_1^{-1}(p') \in U_1$ and $p_2 = T_2^{-1}(p') \in U_2$. This means that two points $p_1 \in U_1$ and $p_2 \in U_2$, located at opposite sides with respect to $\widehat{CS}_{-1}$, are mapped in the same side with respect to $\widehat{CS}$, in the region Z_{k+2}. This is also expressed by saying that the ball U is "folded" by T along $\widehat{CS}$ on the side with more preimages. The same concept can be equivalently expressed by stressing the "unfolding" action of T^{-1}, obtained by the application of the two distinct inverses in Z_{k+2} which merge along $\widehat{CS}$, because if we consider a ball $V \subset Z_{k+2}$, then the set of its $rank - 1$ preimages $T_1^{-1}(V)$ and $T_2^{-1}(V)$ is made up of two balls $T_1^{-1}(V) \in R_1$ and $T_2^{-1}(V) \in R_2$, and these balls are disjoint if $V \cap \widehat{CS} = \emptyset$.

This is the basic reason for the existence of nonconnected basins, a property specific to noninvertible maps. We recall that the *basin* of an attractor A is the set of all the

5

points that generate trajectories converging to A

$$\mathcal{B}(A) = \left\{ x | T^k(x) \rightarrow A \quad as \ k \rightarrow +\infty \right\} \tag{2}$$

If U is a neighborhood of A whose points converge to A (which exists by definition of attractor) then $U \subseteq \mathcal{B}(A)$, and *also the points which are mapped inside U after a finite number of iterations belong to $\mathcal{B}(A)$*, thus the *basin of A* is formed by all the preimages of the points of U :

$$\mathcal{B}(A) = \bigcup_{j=0}^{\infty} T^{-j}(U) \tag{3}$$

where $T^{-1}(x)$ represents the set of the rank-1 preimages of x (i.e. the points mapped into x by T), and $T^{-j}(x)$ represents the set of the $rank - j$ preimages of x (i.e. the points mapped into x after j applications of T).

Now, let us assume that $\mathcal{B}(A)$ is a connected basin for a given set of parameters, and as a parameter is changed $\mathcal{B}(A)$ has a contact with CS, after which a portion of $\mathcal{B}(A)$, say $\mathcal{B}_H$, crosses CS and enters a region Z_{k+2} with more preimages. This implies the creation of new portions of $\mathcal{B}(A)$ given by the new preimages $T_i^{-1}(\mathcal{B}_H)$, $i = 1, 2$. If these preimages belong to regions Z_k, with $k > 0$, also other portions of $\mathcal{B}(A)$ are created after the contact, given by higher rank preimages of $\mathcal{B}_H$.

To sum up, we may say that the backward iteration of a noninvertible map T *repeatedly unfold* the phase space, and this implies that a basin of attraction may be nonconnected, i.e. formed by several (even infinitely many) disjoint portions. In fact, as a suitable set U in (3), we may take the so called *immediate basin* of an attracting set A, $\mathcal{B}_0(A)$, defined as the widest connected component of the basin which contains A. Then the basin of A (or total basin) is given by the whole set of preimages, of any rank, of the immediate basin:

$$\mathcal{B}(A) = \bigcup_{k=0}^{\infty} T^{-k}(\mathcal{B}_0(A)) \tag{4}$$

and, from the arguments given above, it follows that such a set may be made up of infinitely many disjoint components. So, the global bifurcations which transform a simply connected basin into a nonconnected one can be explained in terms of *contacts of basins boundaries and critical sets*. As stressed in the introduction, their study is generally based on both theoretical and computational methods, and, as we shall see in the example discussed below, the *graphical visualization* is often crucial in the discovery and explanation of changes in dynamic scenarios and their parameter dependence.

3 The triopoly game and its equilibria

The time evolution of the triopoly game proposed in [3] is obtained by the iteration of the three-dimensional map $T : (q_1, q_2, q_3) \to (q_1', q_2', q_3')$

$$
T : \begin{cases}
q_1' = (1 - \lambda_1) q_1 + \lambda_1 \mu_1 [q_2 (1 - q_2) + q_3 (1 - q_3)] \\
q_2' = (1 - \lambda_2) q_2 + \lambda_2 \mu_2 [q_3 (1 - q_3) + q_1 (1 - q_1)] \\
q_3' = (1 - \lambda_3) q_3 + \lambda_3 \mu_3 [q_1 (1 - q_1) + q_2 (1 - q_2)]
\end{cases}
\tag{5}
$$

where q_i, $i = 1, 2, 3$, represent the productions at time t of the competing firms which sell the same good in a given market, and q_i' the respective productions at time $t + 1$. The parameters belong to the parameter space

$$
\Omega = \{\mu_i > 0 \text{ and } \lambda_i \in [0, 1]\}
\tag{6}
$$

The fixed points of the map (5), Nash equilibria of the game, are solutions of the following algebraic system of degree 8

$$
\begin{aligned}
\mu_1 [q_2 (1 - q_2) + q_3 (1 - q_3)] &= q_1 \\
\mu_2 [q_1 (1 - q_1) + q_3 (1 - q_3)] &= q_2 \\
\mu_3 [q_2 (1 - q_2) + q_1 (1 - q_1)] &= q_3
\end{aligned}
\tag{7}
$$

It is evident that the point $E_1 = (0, 0, 0)$ is always a fixed point, so at least another real solution of (7) must exist. As shown in [3], a complete analytical solution of the system (7) can be found under the assumption

$$
\mu_1 = \mu_2 = \mu_3 = \mu.
\tag{8}
$$

In this case, the second fixed point, which exists for each value of μ, is given by

$$
E_2 = \left(1 - \frac{1}{2\mu}, 1 - \frac{1}{2\mu}, 1 - \frac{1}{2\mu}\right).
$$

and other six fixed points exist provided that $\mu > \sqrt{2} + \frac{1}{2}$, given by

$$
\begin{aligned}
E_3 &= \left(\frac{1+2\mu+\sqrt{\Psi}}{4\mu}, \frac{1+2\mu+\sqrt{\Psi}}{4\mu}, \frac{3+2\mu-\sqrt{\Psi}}{4\mu}\right) & E_4 &= \left(\frac{1+2\mu-\sqrt{\Psi}}{4\mu}, \frac{1+2\mu-\sqrt{\Psi}}{4\mu}, \frac{3+2\mu+\sqrt{\Psi}}{4\mu}\right) \\
E_5 &= \left(\frac{3+2\mu-\sqrt{\Psi}}{4\mu}, \frac{1+2\mu+\sqrt{\Psi}}{4\mu}, \frac{1+2\mu+\sqrt{\Psi}}{4\mu}\right) & E_6 &= \left(\frac{3+2\mu+\sqrt{\Psi}}{4\mu}, \frac{1+2\mu-\sqrt{\Psi}}{4\mu}, \frac{1+2\mu-\sqrt{\Psi}}{4\mu}\right) \\
E_7 &= \left(\frac{1+2\mu+\sqrt{\Psi}}{4\mu}, \frac{3+2\mu-\sqrt{\Psi}}{4\mu}, \frac{1+2\mu+\sqrt{\Psi}}{4\mu}\right) & E_8 &= \left(\frac{1+2\mu-\sqrt{\Psi}}{4\mu}, \frac{3+2\mu+\sqrt{\Psi}}{4\mu}, \frac{1+2\mu-\sqrt{\Psi}}{4\mu}\right)
\end{aligned}
$$

where $\Psi = \Psi(\mu) = 4\mu^2 - 4\mu - 7$. A complete study of the local stability properties is easily obtained in the symmetric case of identical competing firms, i.e.

$$\lambda_1 = \lambda_2 = \lambda_3 = \lambda. \tag{9}$$

as stated in the following proposition (see [3])

Proposition. *Let (8) and (9) hold. Then*

(i) the fixed point E_1 exists for each $(\mu, \lambda) \in \Omega$ and it is a stable node for $(\mu, \lambda) \in \Omega^s(E_1)$, with $\Omega^s(E_1) = \left\{ (\mu, \lambda) \in \Omega \mid \mu < \frac{1}{2} \right\}$;

(ii) the fixed point E_2 exists for each $(\mu, \lambda) \in \Omega$ and it is a stable node for $(\mu, \lambda) \in \Omega^s(E_2)$, with $\Omega^s(E_2) = \left\{ (\mu, \lambda) \in \Omega \mid \frac{1}{2} < \mu < 2 \text{ and } \lambda(2\mu - 1) < 2 \right\}$;

(iii) the fixed points E_3, E_5 and E_7 exist for $\mu \geq 1/2 + \sqrt{2}$ and are always unstable;

(iv) the fixed points E_4, E_6 and E_8 exist for $\mu \geq 1/2 + \sqrt{2}$ and are stable for $(\mu, \lambda) \in \Omega^s(E_4) = \Omega_1^s(E_4) \cup \Omega_2^s(E_4)$, with

$$\Omega_1^s(E_4) = \left\{ (\mu, \lambda) \in \Omega \mid \frac{1}{2} + \sqrt{2} < \mu < 2 \text{ and } 0 < \lambda < \lambda_f(\mu) \right\}$$

and

$$\Omega_2^s(E_4) = \left\{ (\mu, \lambda) \in \Omega \mid \mu > 2 \text{ and } 0 < \lambda < \lambda_h(\mu) \right\}$$

where $\lambda_f(\mu)$ and $\lambda_h(\mu)$ are given by

$$\lambda_f(\mu) = \frac{8}{5 - \sqrt{\Psi(\mu)} + \sqrt{\left(25 + 7\sqrt{\Psi(\mu)}\right)\left(1 - \sqrt{\Psi(\mu)}\right)}} \tag{10}$$

and

$$\lambda_h(\mu) = \frac{5 - \sqrt{\Psi(\mu)}}{\sqrt{\Psi(\mu)}\left(\sqrt{\Psi(\mu)} + 1\right)} \tag{11}$$

respectively. In the region $\Omega_1^s(E_4)$, E_4, E_6 and E_8 are stable nodes, in the region $\Omega_2^s(E_4)$ they are stable foci.

From this proposition it follows that a wide range of parameters exists which gives *coexistence of stable Nash equilibria*. Since the stability regions $\Omega^s(E_2)$ and $\Omega^s(E_4)$ overlap for $\frac{1}{2} + \sqrt{2} < \mu < 2$ and $\lambda(2\mu - 1) < 2$ in such a region we have four coexisting Nash equilibria, E_2, E_4, E_6 and E_8, which are stable
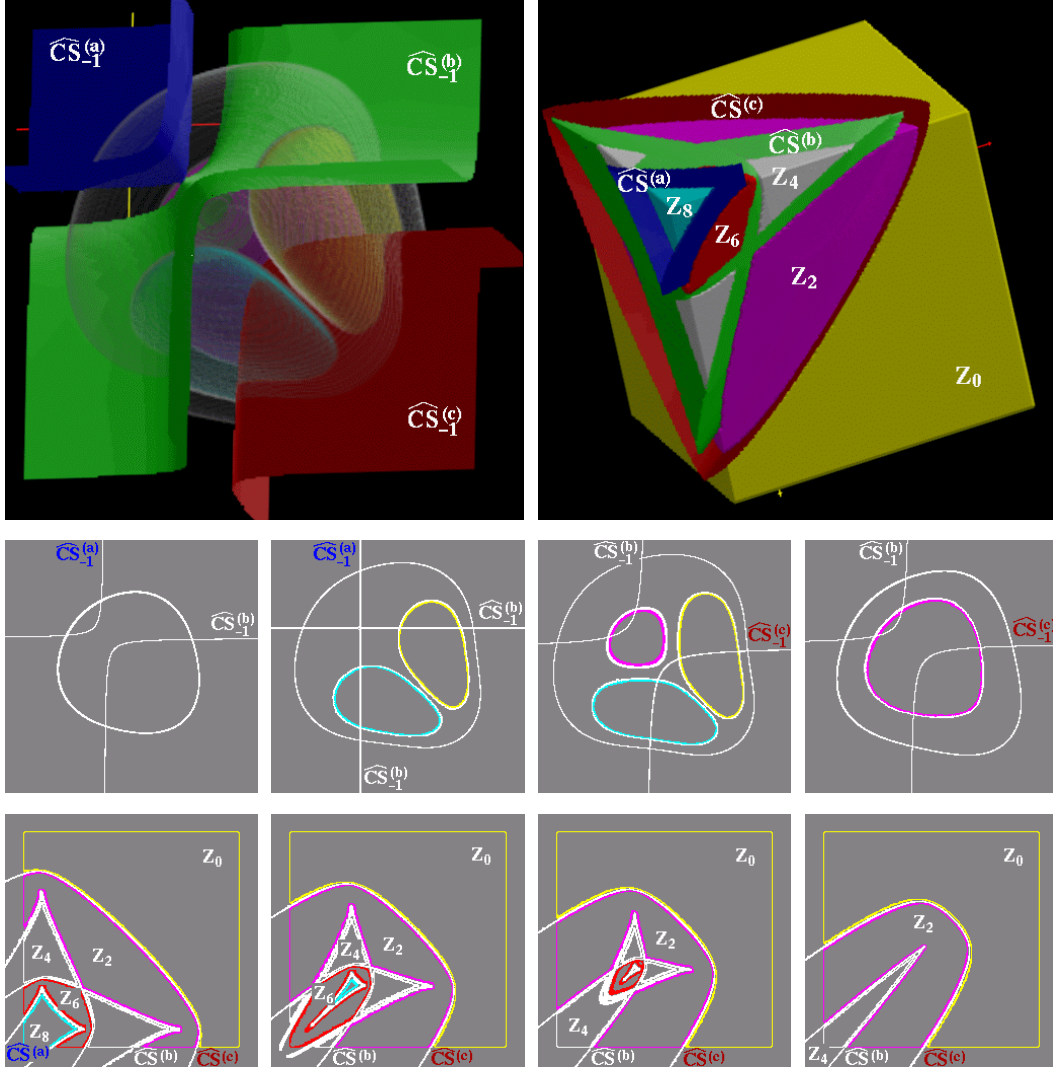
Fig. 2. CS_{-1} (top left image, three sheets $CS_{-1}^{(a)}$, $CS_{-1}^{(b)}$, and $CS_{-1}^{(c)}$, depicted together with basins of attraction) and CS (top right image, three sheets $CS^{(a)}$, $CS^{(b)}$, and $CS^{(c)}$, depicted together with separated zones Z_0, Z_2, Z_4, Z_6, and Z_8) visualized in 3D – the images below the top row show planar intersections at different (increasing) depth values for both 3D illustrations.

nodes. In the portion $\Omega_2^s(E_4)$ of the region $\Omega^s(E_4)$ we have the three coexisting stable Nash equilibria E_4, E_6 and E_8, which are stable foci, and in the portion $\Omega_1^s(E_4)$ of $\Omega^s(E_4)$ with $\frac{1}{2} + \sqrt{2} < \mu < 2$ and $\lambda(2\mu - 1) > 2$ the three stable Nash equilibria E_4, E_6 and E_8 exist, which are stable nodes. Accordingly, the questions stated in the introduction naturally arise, namely, to which Nash equilibrium does the evolutionary process described by the market dynamics lead and which role do the initially chosen quantities of the competitors play in this process? An answer to this question requires a global analysis of the map (5), which is a three-dimensional *noninvertible map*. Indeed, given a point (q_1', q_2', q_3') its rank-1 preimages $T^{-1}(q_1', q_2', q_3')$, may be more than one (really up to eight) since they are obtained by solving the eighth degree algebraic system (5) with respect to the

unknowns (q_1, q_2, q_3). For this map, which is continuously differentiable, we have $CS_{-1} = \{(q_1, q_2, q_2) \in \mathbb{R}^3 \,|\, \det DT = 0\}$, where

$$DT(q_1, q_2, q_2) = \begin{bmatrix} 1 - \lambda_1 & \mu_1\lambda_1(1 - 2q_2) & \mu_1\lambda_1(1 - 2q_3) \\ \mu_2\lambda_2(1 - 2q_1) & 1 - \lambda_2 & \mu_2\lambda_2(1 - 2q_3) \\ \mu_3\lambda_3(1 - 2q_1) & \mu_3\lambda_3(1 - 2q_2) & 1 - \lambda_3 \end{bmatrix} \qquad (12)$$

and the critical set CS, which separates regions with different numbers of rank-1 preimages, is obtained as $CS = T(CS_{-1})$. Three-dimensional pictures of the sets CS_{-1} and CS, as well as their projections on the coordinate planes are shown in Fig. 2. It can be noticed that the critical set CS subdivides the phase space into the regions Z_0, Z_2, Z_4, Z_6, Z_8, nested one into the other, with the points far from the origin $O = (0, 0, 0)$ belonging to Z_0, as can be easily seen from the algebraic system (5) when solved with respect to the unknowns q_i with sufficiently high values of q_i'.

4 Graphical study of the contact bifurcations

For a proper visual investigation of the bifurcation event, which leads to the creation of disjoint parts of a basin of attraction, two types of structures within the phase space need to be visualized. First, the boundary of each basin of attraction has to be depicted. Secondly, CS and the way it subdivides the phase space into regions with different numbers of preimages (zones Z_i) has to be depicted. Unlike the 2D case, in 3D this is not a trivial task – basin boundaries may be of complex shape themselves and/or be grouped in a hierarchical way such that they are spatially stacked over each other. Moreover, CS may consist of several sheets folded over each other in a complex way. Visualization of such 3D structures poses the problem of occlusion, which is dealt with by rendering selected parts of the 3D objects with different levels of transparency.

The standard procedure of representing surfaces in interactive computer graphics is to use of an approximation of the surface, which is constructed from many tiny triangles (see [19]). This surface representation can usually be rendered in an efficient way, by exploiting acceleration hardware widely available in current PCs. Unfortunately, due to the often complex shape of basin boundaries and critical sets, tremendous amounts of triangles would be needed for a proper approximation of the 3D structures, resulting in a rather weak rendering performance (several seconds per image). Contrarily, visualization applications designed for interactive use require update rates no slower than 10Hz.

To allow interactive viewing and manipulation we use a volumetric representation of investigated structures instead of triangles, which – in our case – can be

rendered interactively (see [17,25]). An axis-parallel box-shaped sub-set of phase space − $[x_{min}, x_{max}] \times [y_{min}, y_{max}] \times [z_{min}, z_{max}]$ − which contains all the structures of interest is discretized (sampled) to a regular 3D grid (volume data-set). Each structure (basin boundary or critical set) is represented by a set of samples (called *voxels*) within the volume. A voxel can belong to several structures (to CS and a basin boundary for example).

The visualization process is subdivided into two stages. First, during a time-consuming preprocessing step, the discretized representation of the boundaries and the critical set is computed off-line. The computation results in a data-file, which afterwards can be viewed and interactively investigated during the second step. The system in use actually processes a 4D data-set before rendering, because the parameter responsible for the bifurcation of interest is also discretized to several values before and after the bifurcation.

To obtain the boundaries of basins within the investigated portion of phase space, a trajectory is started at the center of each voxel v. After determining to which attractor E_j the trajectory converges, the voxel is labelled as belonging to the basin $\mathcal{B}(E_j)$. After classifying all voxels of the volume data, the boundary of $\mathcal{B}(E_j)$ is determined as the set of all voxels v which have at least one neighbor which itself belongs to another basin than v. If the coordinates of v within the volume data-set are x, y, and z, there are 26 neighbors with coordinates $(x + dx, y + dy, z + dz)$, where dx, dy, dz assume the values $\{-1, 0, 1\}$, except for $dx = dy = dz = 0$.

For the calculation of CS the determinant of the Jacobian matrix is evaluated at the center of each voxel. If the sign of the determinant differs for two neighboring voxels, CS_{-1} is assumed to pass in-between. If required, the voxels close to CS_{-1} can be marked for serving as a representation of CS_{-1} during visualization. For acquiring a voxel of the representation of CS, binary subdivision is performed in-between the two voxels to obtain a more precise location of CS_{-1}. The image by T of this point of CS_{-1} gives a voxel of CS. Further iterations can be performed to build up representations of $CS_1 = T(CS), \ldots, CS_n = T^n(CS)$ successively.

As – in the current application – we are interested in contacts between basin boundaries and CS, the visualization of the distance between voxels of CS and the closest voxel of a boundary is useful. Distance information can be associated with each voxel of CS and displayed during visualization. The distance computation is performed using 3D distance metric which is a close and fast approximation of the shortest Euclidean distance to a set of voxels (see [28]).

As only the contacts between a basin boundary and specific parts of CS result in the creation of disjoint basins, CS has to be further subdivided into several objects, because uninteresting parts of CS can be omitted during visualization to reduce occlusion and the complexity of the resulting image.

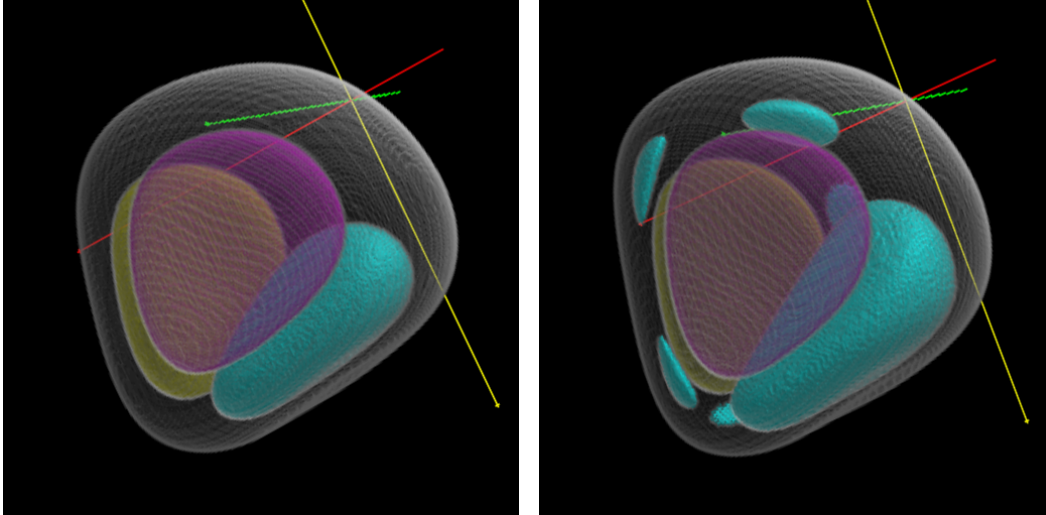Volume rendering ([18]) is used for the visualization of the data obtained after the

Fig. 3. Basins of attraction (four attractors except ∞) visualized before and after the contact bifurcation – the creation of disjoint parts of one basin (depicted in cyan) is clearly visible.

computation step. Basic volume rendering interprets the contents of a scalar data volume as densities of a medium (similar to gas or particles) with specific optical absorption and emission properties (see [20]). An image is produced by integrating the contributions of the medium along viewing rays shot through each pixel of the image. In practise, the integration is replaced by summing up samples of contributions along the viewing ray, see [16]. This simple model can be used for depicting cloud-like 3D objects like fog or fire. More sophisticated approaches make use of transfer functions (see [18]) allowing for arbitrary assignment of optical properties to data values. The most well-known images obtained using this technique are probably images from medical applications (bones together with soft tissue around) obtained from computed tomography data (CT) or similar acquisition devices. By assigning different colors to voxels belonging to different objects, distinction between objects is accomplished. Assigning different absorption levels to different objects, allows to see through them to perceive structures nested within them – for example basin boundaries within basin boundaries.

To achieve a better impression of the 3D shape and spatial correlation of the objects, the influence of a light source onto the color of each voxel is also included during rendering [26]. To ease the visual detection of parts of CS where the contact event takes place, the distance to the nearest basin boundary, which has been computed during the first step, can be used to modify either the color, or the transparency of each voxel of CS. Thus, the closest areas of the critical set can be either highlighted by coloring them red, for example, or parts of CS which are far away from any basin boundary can be rendered more or less transparent, reducing the complexity of the image and depicting only possibly important parts of the surface.

Especially for the investigation of bifurcation events, several data-sets for different settings of the bifurcation parameter have been computed. Using our viewer, which
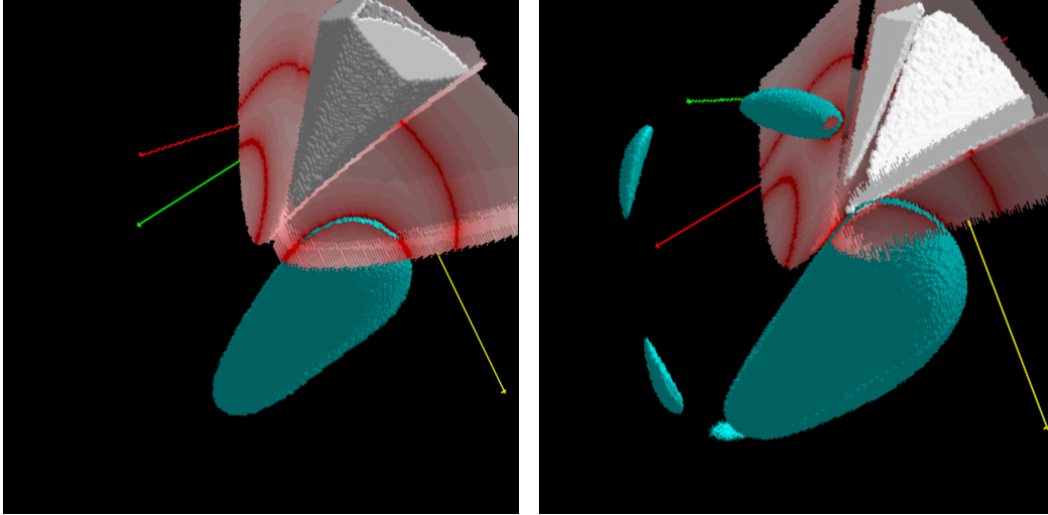
12

Fig. 4. The basin of attraction which causes the contact bifurcation is visualized in 3D together with reponsible parts of CS.

is capable of interactive volume rendering, see [15], the sequence of data-sets can be investigated. By changing the optical properties of voxels belonging to distinct objects, an exploration of the computed data is possible. In the case of basins, only the boundary is depicted. To reduce occlusion, inner parts of a basin are assumed to be totally transparent. As for the given parameter settings the system investigated in this paper exhibits four partly nested basins and a CS folded in a complex way (see Fig. 2), it is crucial to omit nonrelevant objects from rendering in order to obtain a clear view on the location of the bifurcation. An additional tool for revealing hidden parts of the data set is to use clipping planes which remove data above the plane – to provide insight into data below it.

In order to comment an exemplary case, where a contact bifurcation causes the transformation of a basin from simply connected to a nonconnected set, let us consider a set of parameters for which we have four coexisting stable Nash equilibria, the stable nodes E_2, E_4, E_6 and E_8. In Fig. 3a the different basins are represented by different colors [3] : the basins of E_4, E_6, and E_8 are represented by cyan, yellow, and purple, respectively, are nested inside the basin of E_2, whose boundary appears as a semi-transparent surface. The outer (black) region represents the *basin of infinity* $\mathcal{B}(\infty)$, defined as the open set of points that generate diverging trajectories

$$\mathcal{B}(\infty) = \left\{ (q_1, q_2, q_3) \mid \quad \left\| T^t (q_1, q_2, q_3) \right\| \to \infty \text{ as } t \to +\infty \right\} .$$

In Fig. 3a, obtained with parameters' values $\lambda_1 = \lambda_2 = \lambda_3 = 0.5$, and $\mu = 1.95$, the basins $\mathcal{B}(E_4)$, $\mathcal{B}(E_6)$ and $\mathcal{B}(E_8)$ are simply connected sets, and $\mathcal{B}(E_2)$ is a multiply connected set surrounding them. After a small change of the parameters, a qualitatively different structure of the basin $\mathcal{B}(E_4)$ is obtained, as shown in Fig. 3b,

---

[3] for color images refer to URL
http://bandviz.cg.tuwien.ac.at/basinviz/disjoint/

13

obtained with $\lambda_1 = 0.4263$, $\lambda_2 = 0.5$, $\lambda_3 = 0.5737$, and $\mu = 1.95$. Evidently, this slight variation of the parameters caused the occurrence of a global bifurcation at which the basin $\mathcal{B}(E_4)$ becomes a nonconnected set, formed by the so called immediate basin, defined as the larger connected portion of a basin which includes the attractor itself, and several disjoint portions (also called "islands" in [24]), some of which are clearly visible in Fig. 3b.

Other smaller "islands" are also created at the bifurcation, and can be seen by zooming in. The occurrence of this global bifurcations is caused by a contact between the boundary of $\mathcal{B}(E_4)$ and a critical surface, after which a portion of the immediate basin enters a zone characterized by a larger number of preimages, as explained in Section 2. The disjoint portions of $\mathcal{B}(E_4)$ which are clearly visible in Fig. 3b are rank-1 preimages, located across CS_{-1}, of the portion $\mathcal{B}_c$ of the immediate basin which crossed the critical set at the bifurcation, and if some of these "islands" are, at least partially, included inside a zone Z_k with $k > 0$ then other smaller islands are present, which are rank-2 preimages of $\mathcal{B}_c$, and so on.

In order to study the contact which causes such a remarkable basin bifurcation, graphical representations of $\mathcal{B}(E_4)$, together with the critical sets CS, are given in Fig. 4 before and after the contact respectively. The value of the parameters at which the contact occurs, as well as the point of the phase space where the contact occurs, can be easily numerically bounded to the interval $[(0.438, 0.562), (0.44, 0.56)]$ for equally increasing/decreasing values of λ_1 and λ_3; λ_2 equals 0.5 and $\mu = 1.95$. Moreover, the fact that a bifurcation is going to occur can be anticipated because, if required by the user, the computer program calculates the minimal distance between a given basin boundary and the critical set CS, and the points of the basin boundary where such a distance is becoming smaller and smaller can be colored in order to emphasize where the contact is going to occur. This enables one to realize that a qualitative change of the basins structure is going to occur even if the contact point is located behind, and consequently the user can interactively rotate the coordinate axes in order to understand more clearly the kind of contact bifurcation.

Really, the few images given above give a very poor information about the method used to detect the contact bifurcation by using the interactive graphical program. Indeed, the study can only be performed by the usage of animated sequences with the possibility of interactive rotation and transparency modulation of the objects appearing on the screen, as well as a proper interactive usage of cutting planes. Further images, and some animated sequences, can be found at the web page correlated to this work (see [1]).

References

[1] Related web page: http://bandviz.cg.tuwien.ac.at/basinviz/disjoint/.

[2] R. Abraham, L. Gardini and C. Mira, *Chaos in discrete dynamical systems (a visual introduction in two dimension)*, Springer-Verlag, 1997.

[3] H.N. Agiza, G.I. Bischi and M. Kopel "Multistability in a Dynamic Cournot Game with Three Oligopolists", *Mathematics and Computers in Simulation*, 51 (1999) pp.63-90

[4] K. Binmore, Fun and Games, D.C. Heath & C. (1992).

[5] G.I. Bischi and M. Kopel "Equilibrium Selection in a Nonlinear Duopoly Game with Adaptive Expectations", *Journal of Economic Behavior and Organization*, in press.

[6] G.I. Bischi and L. Gardini, "Role of invariant and minimal absorbing areas in chaos synchronization", *Physical Review E*, vol.58 n.5 (1998) pp. 5710-5719.

[7] G.I Bischi, C. Mammana and L. Gardini "Multistability and cyclic attractors in duopoly games", *Chaos, Solitons & Fractals*, 11 (2000) pp. 543-564

[8] G.I. Bischi, L. Gardini and M. Kopel "Analysis of Global Bifurcations in a Market Share Attraction Model", *Journal of Economic Dynamics and Control* , 24, pp. 855-879 (2000).

[9] A. Cournot, *Recherches sur les principes matematiques de la theorie de la richesse*, Hachette, Paris (1838).

[10] D. Friedman "Evolutionary Games in Economics", *Econometrica*, 59 (1991) pp. 637-666.

[11] Fudenberg, D. and Levine, D. (1998): The Theory of Learning in Games, MIT Press.

[12] L. Gardini, R. Abraham, R. Record and D. Fournier-Prunaret, "A double logistic map", *International Journal of Bifurcations and Chaos*, 4, n.1 (1994) 145-176.

[13] J. Guckenheimer and P. Holmes. *Nonlinear Oscillations, Dynamical Systems, and Bifurcations of Vector Fields* (Springer-Verlag, 1983).

[14] I. Gumowski and C. Mira, *Dynamique Chaotique* (Cepadues Editions, Toulose, 1980).

[15] H. Hauser, L. Mroz, G. I. Bischi and M. E. Gröller, "Two-level volume rendering – fusing MIP and DVR", *Proceedings of IEEE Visualization 2000*, Salt Lake City, Utah, 2000, in press.

[16] J. T. Kajiya "Ray Tracing Volume Densities", *Proceedings of ACM SIGGRAPH'84*, (1984) pp. 165-174.

[17] P. Lacroute and M. Levoy, "Fast Volume Rendering Using a Shear-warp Factorisation of the Viewing Transform", *Proceedings of ACM SIGGRAPH '94* (1984), pp. 451–459

[18] M. Levoy, "Display of Surfaces from Volume Data", *IEEE Computer Graphics & Applications*, vol. 8, n. 5 (1988) pp. 29–37.

[19] W. E. Lorensen and H. E. Cline, "Marching Cubes: A High Resolution 3{D} Surface Construction Algorithm", *Proceedings of ACM SIGGRAPH'87* (1987) pp. 163–189.

[20] N. Max, "Optical Models for Direct Volume Rendering", *IEEE Transactions on Visualization and Computer*, vol. 1, n.2 (195) pp. 99–108.

[21] C. Mira, *Chaotic Dynamics*, Word Scientific (1987).

[22] C. Mira and C. Rauzy, Fractal aggregation of basin islands in two-dimensional quadratic noninvertible maps, *International Journal of Bifurcations and Chaos*, vol.5, n.4, 1995, 991-1019.

[23] C. Mira, L. Gardini, A. Barugola and J.C. Cathala, *Chaotic Dynamics in Two-Dimensional Noninvertible Maps*, World Scientific, Singapore, 1996.

[24] C. Mira, D. Fournier-Prunaret, L. Gardini, H. Kawakami and J.C. Cathala "Basin bifurcations of two-dimensional noninvertible maps: fractalization of basins", *International Journal of Bifurcation and Chaos*, 4 (1994) 343-381

[25] L. Mroz and A. König and E. Gröller, "Real Time Maximum Intensity Projection" in *Data Visualization '99*, Proceedings of the Joint EUROGRAPHICS - IEEE TCCG Symposium on Visualization, in press.

[26] B.-T. Phong, "Illumination for computer generated pictures", *CACM*, vol. 18, no. 6, pp. 311–317, June 1975.

[27] J.W. Weibull, *Evolutionary Game Theory*, The MIT Press, 1995

[28] K. Zuiderveld, A. H. J. Koning, and M. A. Viergever, "Acceleration of Ray Casting using 3d Distance Transforms", in Proceedings of Visualization in Biomedical Computing 1992, pp. 324–335, 1992